Research Square

Preprints are preliminary reports that have not undergone peer review.
They should not be considered conclusive, used to inform clinical practice,
or referenced by the media as validated information.

Evolution of the pore structure of activated coal-based activated carbon following activation pretreatment and its phased inhibition effect on spontaneous combustion

Qin Xu
Shanghai Polytechnic University
Yiping Tan
Shanghai Polytechnic University
Jie Guan
Shanghai Polytechnic University
Hao Yuan
Shanghai Polytechnic University
Shengqiang Yang
shengqiangyang@hotmail.com
China University of Mining and Technology
Yaoguang Guo
Shanghai Polytechnic University

Research Article

Keywords: Coal-based activated carbon, Activation pretreatment、Pore structure、Spontaneous combustion、Inhibition

Posted Date: November 23rd, 2026

DOI: https://doi.org/10.21203/rs.3.rs-11539071/v1

License: This work is licensed under a Creative Commons Attribution 4.0 International License.
Read Full License

Additional Declarations: No competing interests reported.

Evolution of the pore structure of activated coal-based activated carbon following activation pretreatment and its phased inhibition effect on spontaneous combustion

Qin Xu[a], Yiping Tan[a], Jie Guan[a*], Hao Yuan [a], Shengqiang Yang[b,**] , Yaoguang Guo[a]

[a] School of Resources and Environmental Engineering, Shanghai Polytechnic University, Shanghai, China.

[b] School of Safety Engineering, China University of Mining and Technology, Xuzhou, China.

Abstract

Coal-based activated carbon is porous and easily oxidized. Under stacking conditions, it is prone to heat-storage oxidation and spontaneous combustion, which are dangerous. This study investigated the effects of particle size and H_3PO_4/CH_3COOK ratio on the pore structure development of coal-based activated carbon. The activated carbon with the most developed pore structure was subsequently treated with $Na_2S_2O_8$ solutions at different concentrations to evaluate the inhibition performance of $Na_2S_2O_8$ and to verify changes in pore structure during the inhibition process. The results showed that the adsorption capacity of activated carbon increased with decreasing particle size and first increased, then decreased, as the H_3PO_4/CH_3COOK ratio increased. The 0–0.074 mm sample activated at an H_3PO_4/CH_3COOK ratio of 1:3 exhibited the most developed

* Corresponding author.

E-mail address: guanjie@sspu.edu.cn (J. Guan)

** Corresponding author.

E-mail address: shengqiangyang@hotmail.com (S. Yang)

pore structure and the highest adsorption capacity. That sample was treated with $Na_2S_2O_8$ at different concentrations. Among them, a 5% $Na_2S_2O_8$ yielded the best inhibition results, increasing the ignition temperature by 33.4℃and reducing the total heat release by 67.68 J/g. Under 5% $Na_2S_2O_8$ treatment, both heat release and mass loss during the oxidative heat accumulation and combustion phases were minimized, while the ignition temperature during the oxidative pyrolysis phase reached its maximum, and the activation energy for each stage was maximized. Furthermore, 5% $Na_2S_2O_8$ maintained a high adsorption capacity while passivating active sites. However, excessive concentration can cause micropores and mesopores to coalesce, destroying the pore structure of activated carbon and reducing adsorption capacity. This study supports the safe storage, transportation, and application of coal-based activated carbon.

Keywords: Coal-based activated carbon；Activation pretreatment；Pore structure；Spontaneous combustion；Inhibition

1 Introduction

China is the world's largest producer and consumer of activated carbon. In 2025, its production reached 980,000 metric tons, accounting for 42% of global output. Of this, coal-based activated carbon production totaled 650,000 metric tons, accounting for 56% of China's total activated carbon output and maintaining a dominant market position1-3. Activated carbon has a highly developed pore structure, a large specific surface area, and strong adsorption capacity, enabling it to purify high-flow, low-concentration exhaust gases; as a result, it is widely used for the adsorption and removal of Volatile Organic Compounds (VOCs)4, 5. Compared with other carbon sources, coal has a high

carbon content, abundant reserves, and a low price. Among coal types, bituminous coal has the largest reserves and the widest distribution, and it possesses a certain degree of initial porosity and moderate carbon skeleton density[6, 7]. Therefore, after carbonization and activation, the resulting coal-based activated carbon has a well-developed pore structure, which increases the surface area available for gas contact and greatly enhances its adsorption performance[8-10]. When VOCs enter the activated carbon adsorption unit, heat generated by adsorption and oxidation causes heat to accumulate. The resulting rise in system temperature accelerates the spontaneous combustion of the activated carbon, which can easily lead to spontaneous combustion fires or even explosions, posing a serious threat to the safe and stable operation of the adsorption unit[11, 12]. Therefore, studying the development of pore structure and the oxidative spontaneous combustion characteristics of coal-based activated carbon after preliminary activation treatment is of great significance for mitigating spontaneous combustion risks associated with activated carbon and ensuring the safe and stable operation of adsorption systems.

To enhance the adsorption performance of coal-based activated carbon, various activation pretreatment methods are often employed to optimize its pore structure[13]. Zhu et . al[1] used Datong bituminous coal as feedstock to prepare coal-based activated carbon through steam activation. The specific surface area increased from 34.7 m^2/g in the raw coal to 724.1 m^2/g, and the pore volume increased from 0.018 cm^3/g in the raw coal to 0.834 cm^3/g, promoting the development of microporous and mesoporous structures. Mousumi et . al[14] used subbituminous coal as feedstock and activated the

activated carbon using ultrasound-assisted KOH and NaOH, resulting in a significant increase in specific surface area from 13.005 m^2/g in the raw coal to 789.910 m^2/g and a significant increase in pore volume from 0.019 cm^3/g in the raw coal to 0.103 cm^3/g.

While the activation pretreatment enhances the pore structure of coal-based activated carbon, it also provides more surface reaction sites for oxygen adsorption and oxidation, thereby generating heat and promoting spontaneous combustion of the activated carbon15. Xiao et . al16 found that both the total heat release and the maximum heat release rate of the activated and carbonized materials were higher than those of the raw coal; both the carbonization and activation processes increased the tendency of the activated carbon to self-ignite. Lyu et . al17 found that carbonization and activation significantly promote the development of the pore structure in coal-based activated carbon, enhance its oxygen adsorption capacity, cause a lag in the overall exothermic process, and reduce the thermal diffusivity and thermal conductivity, thereby increasing the tendency of coal-based activated carbon to spontaneously combust. The above studies indicate that activation pretreatment, while optimizing the pore structure of coal-based activated carbon, also increases its tendency to spontaneously combust. Few studies have examined the relationship between the evolution of pore structure caused by activation pretreatment and the characteristics of oxidative spontaneous combustion; in particular, there is a lack of research exploring how to reduce the risk of spontaneous combustion in coal-based activated carbon while maintaining its pore structure.

Therefore, this study used bituminous coal from Weining County, Guizhou

Province, China, as the raw material to prepare coal-based activated carbon through activation treatments with different ratios of CH_3COOK and H_3PO_4. A fully automated instrument for specific surface area and pore analysis was used to investigate the effects of particle size and activator ratios on the development of the pore structure of coal-based activated carbon. Based on this, coal-based activated carbon with the most well-developed pore structure was selected and subjected to an inhibition treatment using sodium persulfate ($Na_2S_2O_8$) solutions of varying concentrations. A comprehensive thermal analyzer was used to investigate changes in mass loss, characteristic temperatures, and heat release at various stages of oxidative spontaneous combustion of coal-based activated carbon following inhibition with $Na_2S_2O_8$ solutions at different concentrations. Combining kinetic methods such as Flynn-Wall-Ozawa (FWO) and Madhusudanan-Krishnan-Ninan (MKN), we investigated the effects of $Na_2S_2O_8$ inhibition treatment on the activation energy of oxidative spontaneous combustion in coal-based activated carbon. To ensure that $Na_2S_2O_8$ reduces the tendency of coal-based activated carbon to self-ignite while maintaining a high adsorption capacity, a fully automated specific surface area and pore analysis instrument was used to investigate changes in its pore structure. This study reveals the evolution of the pore structure of coal-based activated carbon following pretreatment and its effectiveness in inhibiting spontaneous combustion. The findings are of great significance for preventing spontaneous combustion hazards in activated carbon and ensuring the safe and stable operation of adsorption systems.

2 Materials and methods

2.1 Experimental samples

In this study, bituminous coal from Weining County, Guizhou Province, China, was selected as the raw material for producing activated carbon. This coal type is classified as a weak-coking coal; the industrial analysis of the coal sample is shown in Fig. 1. A fresh coal sample from the center of a large lump of coal was crushed into particles approximately 5 mm in size and dried in a vacuum oven at room temperature for 24 hours. After drying, store the sample in an airtight container for use in subsequent experiments. Grind the dried coal sample and screen it into four particle size ranges:0.178−0.35 mm,0.125−0.178 mm,0.074−0.125 mm, and 0−0.074 mm.

2.2 Equipment and principles

The experiment used an open-type vacuum-tube electric furnace (model SK-G06123K, manufactured by Tianjin Zhonghuan Electric Furnace Co., Ltd.) to prepare coal-based activated carbon. The instrument has a temperature control accuracy of ±1℃, a rated power of 2.5 kW, a rated voltage of 220V, a rated temperature of 1200℃, reaches the maximum temperature in 60 minutes, and the furnace tube dimensions are 60×1000mm.

The pore structure analysis of activated carbon was performed using a fully automated instrument for specific surface area and pore analysis (Model: BELSORP-max, manufactured by Machikubai, Japan). The instrument's specific surface area measurement range is greater than 0.01 m^2/g (N_2/77 K, Ar/87 K) and greater than 0.0005 m^2/g (Kr/77 K); its pore size analysis range is 0.35 nm to 500 nm; and the

sensor's relative pressure measurement range is 1×10^{-9} to 0.997.

The experiment used the HCT-4 Comprehensive Thermal Analyzer (Beijing Hengjiu Experimental Equipment Co, Ltd.) to simultaneously measure thermogravimetry and heat flux. The instrument is equipped with a mass flow controller that supports automatic switching between two gas channels with stable pressure and flow rates. It has a maximum sample capacity of 5 g, a heating temperature range from room temperature to 1550 ℃, a heating rate ranging from 0.1 ℃/min to 100 ℃/min, and a temperature stability of 0.1 ℃.

2.3 Experimental procedure

As shown in Fig. 1(I), four samples of raw coal with different particle size ranges were weighed and placed in an open-type vacuum tube furnace. At a nitrogen flow rate of 90 mL/min, the samples were heated at 10 ℃/min to 300 ℃, then held at that temperature for 2 hours to complete carbonization. Take 1 mL of an 85% H_3PO_4 solution and add it dropwise to 20 mL of deionized water; then add CH_3COOK powder to prepare activator solutions with H_3PO_4/CH_3COOK mass ratios of 1:1, 1:2, 1:3, and 1:4.The carbonized activated carbon samples were immersed in the aforementioned activator solution for 2 hours, dried at 60℃ for 1.5 hours, and then placed in a vacuum tube furnace. Under a nitrogen flow rate of 90 mL/min, the temperature was raised at 10℃/min to 500℃, and the samples were activated at a constant temperature for 2 hours. After washing the resulting carbon material with water and an alkali solution and drying it, coal-based activated carbon samples were obtained. As shown in Fig. 1(II), approximately 100 mg of the aforementioned coal-based activated carbon sample was weighed and placed into

a clean sample tube. The sample was degassed under vacuum at 200°C for 6 hours to remove physically adsorbed impurities. After the sample tube had cooled to room temperature, its total mass was measured again to determine the actual net weight of the sample following degassing. The sample tube is then mounted on the analysis port of the fully automated specific surface area and porosity analyzer, and the test is initiated using the control software. At liquid-nitrogen temperature (77 K), using nitrogen (N_2) as the adsorbate, samples are automatically injected at predetermined relative pressure points; the equilibrium adsorption amount is recorded, and a nitrogen adsorption-desorption isotherm is plotted.

As shown in Fig. 1(III), $Na_2S_2O_8$ was used as an inhibition agent to prepare $Na_2S_2O_8$ solutions with mass fractions of 1%, 5%, 10%, and 15%. Next, the coal-based activated carbon samples were completely immersed in $Na_2S_2O_8$ solutions of varying concentrations and left to soak for 0.5 h at room temperature. After soaking, the activated carbon samples were filtered, washed until neutral, and dried to produce a series of inhibited activated carbons. As shown in Fig. 1(IV), 10 mg of the activated carbon sample with inhibition was weighed and placed in a small crucible. The crucible was then placed in a simultaneous thermal analyzer and heated from room temperature to 750°C in a dry air atmosphere at a flow rate of 20 mL/min. The heating rates were set to 5, 10, 15, and 20°C/min to obtain TG-DSC curves for the oxidation of coal-based activated carbon from room temperature to 750°C. Finally, following the test procedure shown in Fig. 1(II), the coal-based activated carbon sample treated with an inhibitor was placed in a fully automated instrument for specific surface area and pore analysis.

At liquid-nitrogen temperature (77 K) and using nitrogen (N_2) as the adsorbate, the equilibrium adsorption capacity was measured at predetermined relative pressure points, and nitrogen adsorption-desorption isotherms were plotted.

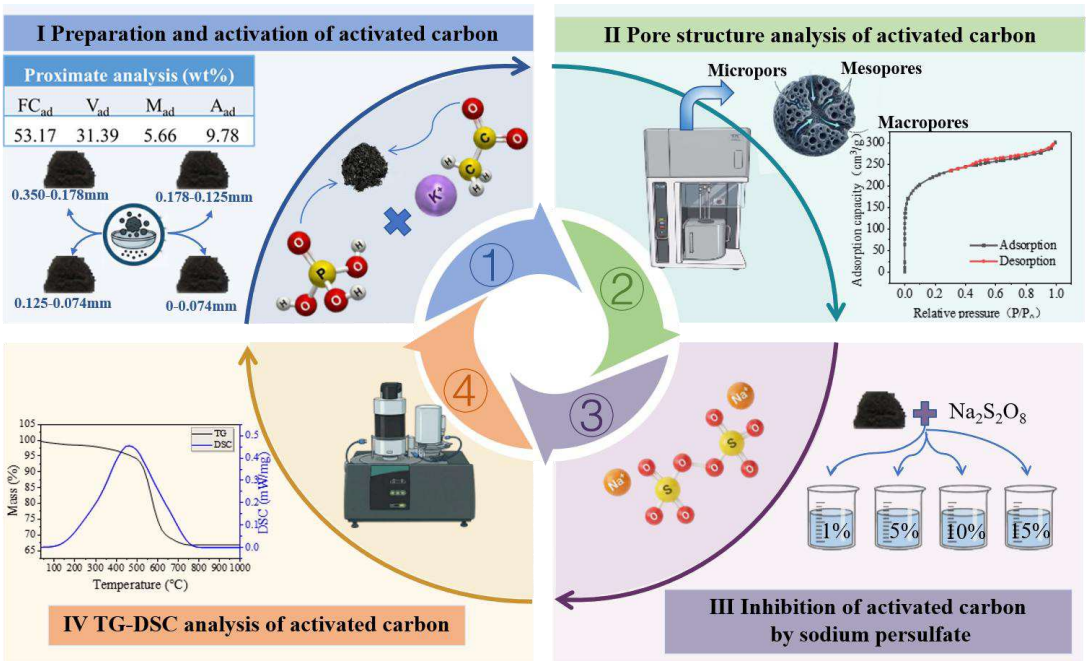


Fig. 1. Schematic diagram of the experimental procedure.

3. Results and discussion

3.1 Changes in pore structure during the activation pretreatment process of coal-based activated carbon

3.1.1 Nitrogen adsorption-desorption isotherms and pore type analysis

As shown in Fig. 2, according to the standards of the International Union of Pure and Applied Chemistry (IUPAC)18, the nitrogen adsorption-desorption isotherms of coal-based activated carbon all exhibit a combination of Type I and Type IV characteristics. In regions of relatively low pressure ($P/P_0<0.1$), the increase in adsorption potential causes the micropores to exhibit extremely strong adsorption of nitrogen molecules,

and the adsorption capacity shows a sharp upward trend19. As the relative pressure increases, the rate of adsorption growth tends to level off. In the moderate relative pressure range (P/P_0>0.4), the adsorption and desorption branches become distinctly separated, forming an H4-type hysteresis loop. Capillary coalescence gradually intensifies, and the nitrogen adsorption process gradually shifts from micropore filling to mesopore filling20.

There are significant differences in the adsorption capacity of coal-based activated carbon across particle sizes, with an overall trend of increasing capacity as raw coal particle size decreases. Specifically, within the particle size range of 0−0.074 mm, coal-based activated carbon exhibited the highest adsorption capacity under all activator ratios, with maximum adsorption capacities exceeding 300 cm^3/g. The smaller the raw coal particle size, the greater the specific surface area, allowing the activator to penetrate more uniformly and thoroughly into the activated carbon, thereby promoting pore development21. Within the same particle size range, as the H_3PO_4/CH_3COOK ratio increased from 1:1 to 1:4, the adsorption capacity of activated carbon first increased and then decreased, with the maximum adsorption capacity observed at a ratio of 1:3. An appropriate activator ratio promotes the development of the pore structure in coal-based activated carbon, but an excessively high ratio leads to excessive erosion of the pore structure, thereby reducing gas adsorption capacity.

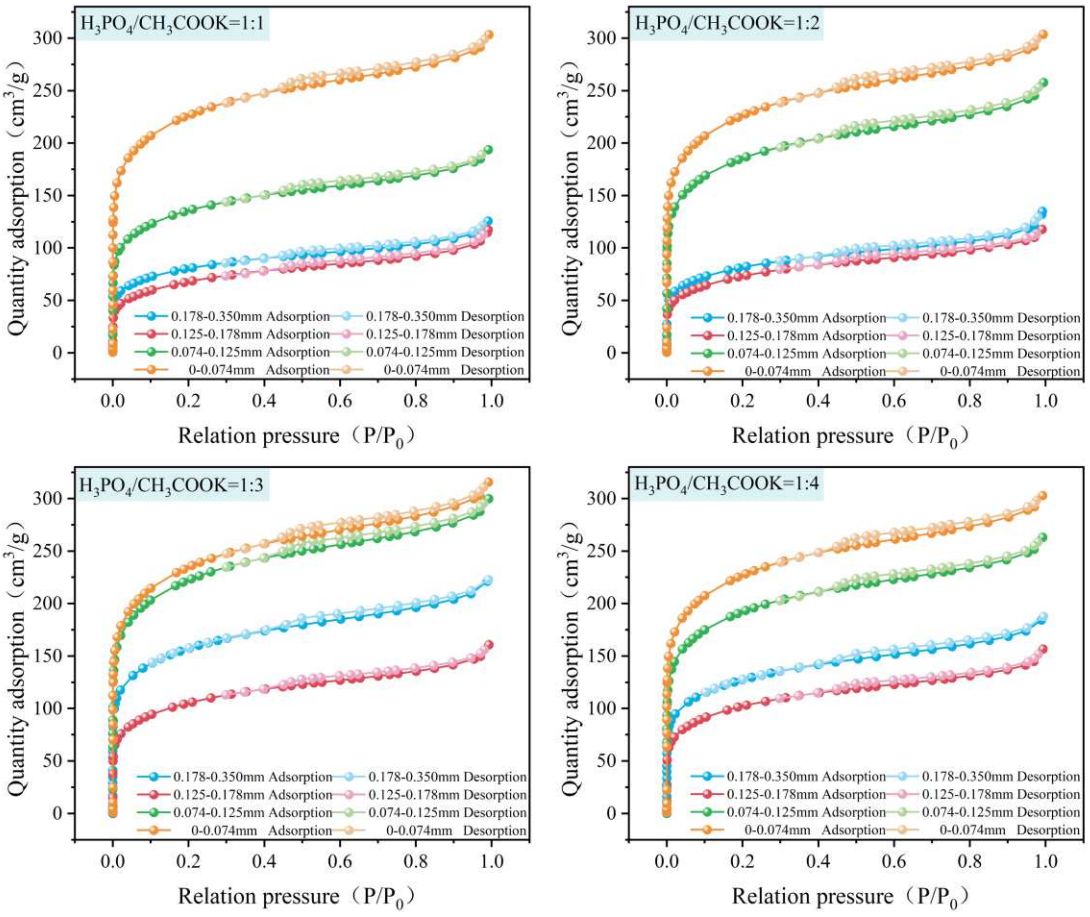


Fig. 2. Nitrogen adsorption-desorption isotherms for coal-based activated carbon.

3.1.2 Analysis of pore size distribution in relation to pore volume and specific surface area

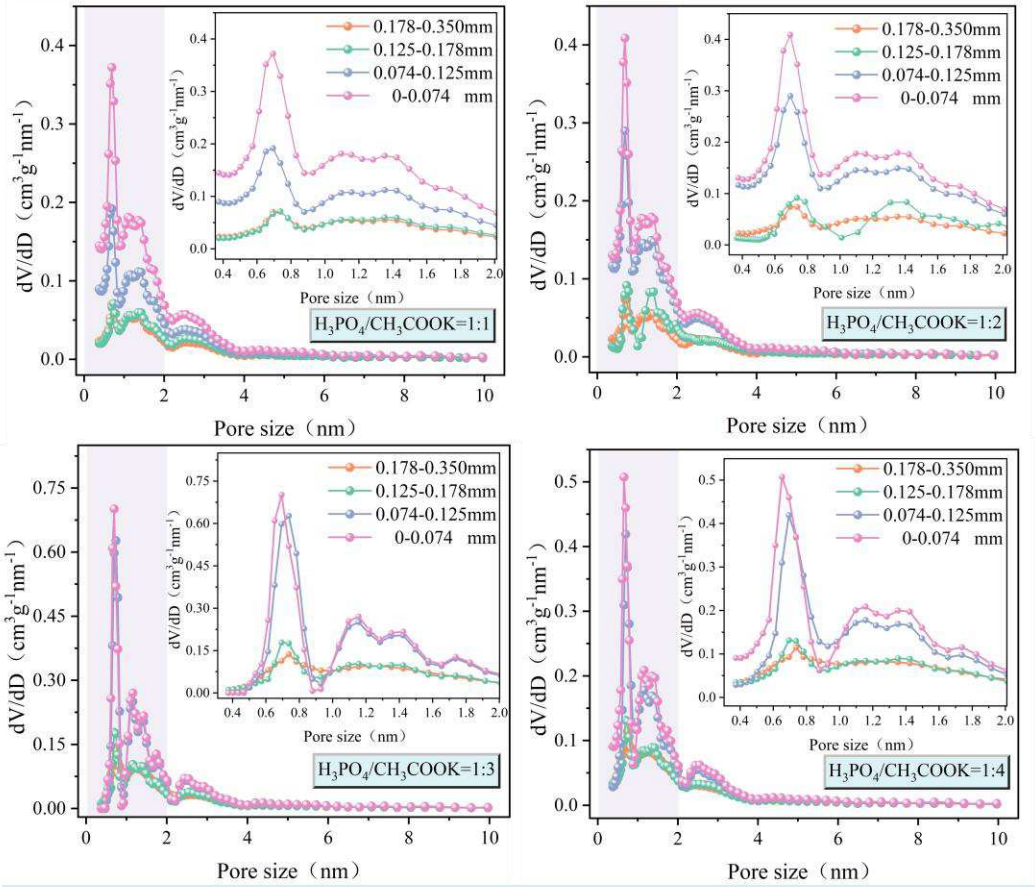
Based on the characteristics of the adsorption-desorption isotherms shown in Fig. 2, coal-based activated carbon contains numerous micropores and exhibits a distinct mesoporous hysteresis loop.

Density Functional Theory (DFT) models can numerically invert N_2 adsorption isotherms, thereby yielding a continuous and accurate pore size distribution over the entire range from ultra-micropores to mesopores (typically 0.4-50 nm)22, 23. Fig. 3 shows the differential distribution curves of pore volume and specific surface area for

coal-based activated carbon obtained using a DFT model. The coal-based activated carbon samples exhibit similar distribution characteristics across different size ranges: a steep and sharp ultra-micropore peak in the 0.6–0.8 nm range, several micropore peaks in the 1–2 nm range, and a gradually flattening curve in the mesopore range of 2–10 nm.

At the same activator ratio, the pore size distributions for the 0.178−0.350 mm and 0.125−0.178 mm particle size ranges exhibited a two-peak distribution, while those for the 0.074−0.125 mm and 0−0.074 mm particle size ranges exhibited a four-peak distribution. At the main peak with a pore size of 0.6−0.8 nm, the mode for pore size tends to shift toward smaller pore sizes as particle size decreases. The reduction in particle size allows the activator to penetrate more rapidly and uniformly, enabling deeper and more precise chemical etching of the carbon matrix. This results in a more developed pore structure in coal-based activated carbon, particularly promoting the development of ultra-micropores. Within the same particle size range, as the H_3PO_4/CH_3COOK ratio increased from 1:1 to 1:4, the intensity of the ultra-micropore peak in both the pore volume derivative curve (dV/dD) and the specific surface area derivative curve (dA/dD) first increased and then decreased; the ultra-micropore peak intensity reached its maximum when the H_3PO_4/CH_3COOK ratio was 1:3. When the H_3PO_4/CH_3COOK ratio increased to 1:4, the intensity of the ultra-micropore peak decreased. An excess of CH_3COOK caused excessive etching of the activated carbon, leading to the merging or even localized collapse of some micropores, which reduced the number of ultra-micropores.

(a) Pore volume differential distribution curves of activated carbon



(b) Pore surface area differential distribution curves of activated carbon

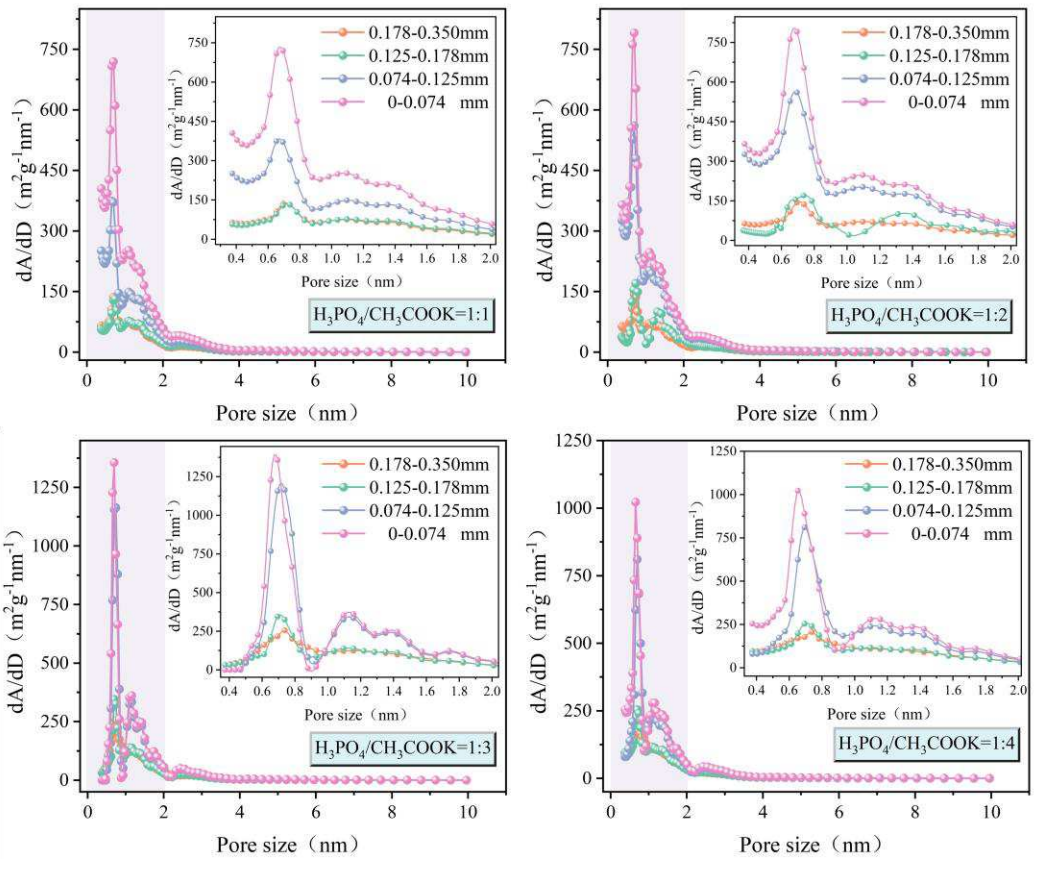


Fig. 3. Pore size distribution curve of coal-based activated carbon.

3.1.3 Analysis of pore volume and specific surface area in micropores, mesopores, and macropores pore structures

As shown in Fig. 4, the pore volume and specific surface area of coal-based activated carbon increase as particle size decreases. Furthermore, smaller particles are heated more uniformly, resulting in better activation and a more developed pore structure. As the H_3PO_4/CH_3COOK ratio increased, the pore volume of the coal-based activated carbon first rose and then fell; at a ratio of 1:3, the pore volume reached its maximum value of 0.3976 cm^3/g. This trend is consistent with the pattern of specific surface area versus the H_3PO_4/CH_3COOK ratio. As the H_3PO_4/CH_3COOK ratio increases, the specific surface area of the coal-based activated carbon first increases and then decreases; at a ratio of 1:3, it reaches a maximum of 805.7 m^2/g. Increasing the H_3PO_4/CH_3COOK ratio can increase the pore volume and specific surface area of coal-based activated carbon; however, an excessively high ratio can damage the carbon precursor, leading to the destruction of the activated carbon's pore structure and a decrease in pore volume and specific surface area.

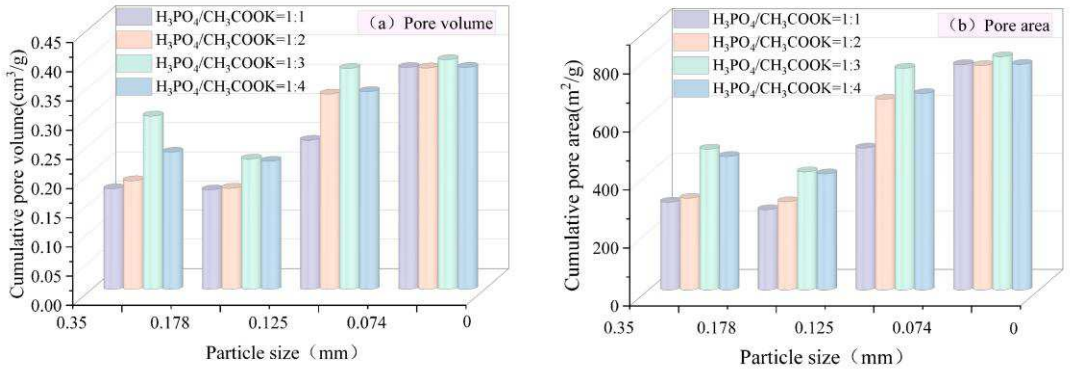


Fig. 4. Cumulative pore volume and cumulative pore Area of coal-based activated carbon.

According to IUPAC standards, the pores in activated carbon are classified as micropores (R_{pore}< 2 nm), macropores (R_{pore} > 50 nm), and mesopores (with pore sizes between the two); these are interrelated and together form a hierarchical pore structure24. The distribution of micropore, mesopore, and macropore volumes and specific surface area in the pore structure of coal-based activated carbon is shown in Fig. 5. When the H_3PO_4/CH_3COOK ratio was 1:1, as the particle size decreased, the specific surface area increased from 303.29 cm^3/g to 777.84 cm^3/g; specifically, the micropore specific surface area increased by 166.51%, the mesopore specific surface area increased by 88.78%, and the macropore specific surface area did not exceed 5 m^2/g; The total pore volume increased from 0.1723 cm^3/g to 0.3802 cm^3/g, with the micropore volume increasing by 168.94% and the mesopore volume by 113.03%, while the macropores volume showed minimal change, remaining below 0.02 cm^3/g. The increase in total pore volume and specific surface area resulted from the growth of micropores and mesopores. Among these, micropores exhibited the greatest increases in specific surface area and pore volume and played a dominant role in the development of the pore structure, while mesopores also showed significant increases in specific surface area and pore volume, which similarly contributed to the development of the pore structure.

At the same particle size, as the H_3PO_4/CH_3COOK ratio increases, both the pore volume and specific surface area of the microporous and mesoporous materials first

increase and then decrease; at a ratio of 1:3, both reach their maximum values. For example, in the particle size range of 0.350-0.178 mm, the microporous specific surface area was highest at a 1:3 activator ratio, reaching 316.68 m^2/g—a 33.99% increase compared to a 1:1 activator ratio—while the mesoporous specific surface area increased by 154.91%; the microporous pore volume increased by 83.31%, and the mesoporous pore volume increased by 85.76%. When the CH_3COOK ratio was further increased to 1:4, the micropore specific surface area decreased to 0.1093 m^2/g, a decline of 8.51%, while the mesopore specific surface area decreased by 6.1%; the micropore pore volume decreased by 25.65%, and the mesopore pore volume decreased by 18.41%; the macropore specific surface area increased by 125.1%, and the pore volume increased slightly. Excessive CH_3COOK led to over-etching of the carbon framework, causing some micropores to merge or local pore channels to degrade, thereby reducing micropore volume and specific surface area while increasing macropore volume and specific surface area.

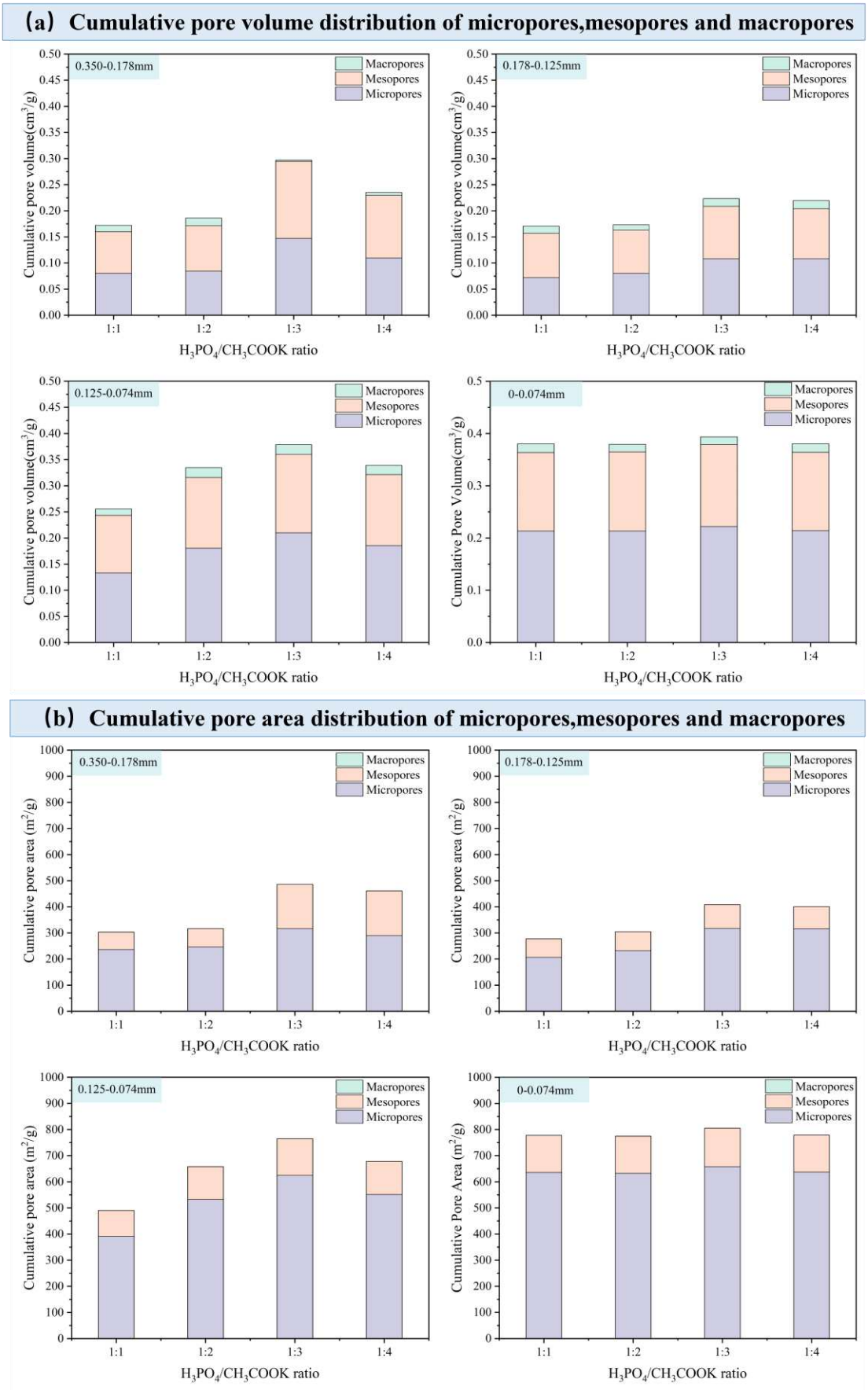


Fig. 5. Distribution of micropore, mesopore, and macropore volumes and surface

areas in the pore structure of coal-based activated carbon.

3.2 Analysis of the inhibition effect of $Na_2S_2O_8$ on the characteristic stages of spontaneous combustion in coal-based activated carbon

As shown in Section 3.1, when the H_3PO_4/CH_3COOK ratio is 1:3, the pore structure of coal-based activated carbon in the 0−0.074 mm particle size range is most well-developed. As an example, the TG-DSC curve and adsorption-desorption curves for this sample are shown in Fig. 6. As shown in Fig. 6(a), there are three characteristic temperature points in the spontaneous combustion process of coal-based activated carbon: T_1 represents the pyrolysis temperature at which heat accumulates in the coal-based activated carbon until oxidative decomposition occurs; T_2 represents the ignition temperature at which combustion begins and the mass decreases rapidly; T_3 represents the combustion-out temperature corresponding to complete combustion. Based on these characteristic temperatures, the spontaneous combustion process of activated carbon—from the low-temperature oxidation stage to complete combustion—is divided into four stages: the oxidative heat accumulation phase (room temperature−T_1), the oxidative pyrolysis phase (T_1−T_2), the combustion phase (T_2−T_3), and the complete combustion phase (>T_3). As the temperature rises, moisture adsorbed within the coal-based activated carbon evaporates, releasing impurities and resulting in a 2.4% mass loss during the oxidative heat accumulation phase. When the temperature exceeds 278℃, a small number of active functional groups in the activated carbon begin to decompose, producing CO and CO_2 gases; the mass loss rate increases, reaching 5.1% during the oxidative pyrolysis phase. When the temperature rises to 508℃, the fixed carbon

framework undergoes vigorous combustion; the mass loss rate and chemical heat release during the combustion phase reach their maximum values, and the DSC curve exhibits a pronounced exothermic peak25. The quality of coal-based activated carbon declines sharply at this stage, with a weight loss rate of up to 26.4%. As the combustible components in the activated carbon are nearly exhausted, the reaction gradually slows and halts around 1000℃. The adsorption-desorption isotherms for coal-based activated carbon are shown in Fig. 6(b); the curves exhibit characteristics of both Type I and Type IV. As can be seen from the particle size distribution curve, the particle size of this activated carbon sample is primarily concentrated in the micropore range. It exhibits one steep and sharp ultra-micropore peak in the 0.6−0.8 nm range, three micropore peaks in the 1−2 nm range, and one broad, gentle, and faint undulating peak in the mesopore range of 2−4 nm; the curve flattens out in the mesopore range of 4−10 nm. The multi-level pore channels of this coal-based activated carbon confer excellent adsorption properties, providing a vast surface area for reactions and facilitating oxidation, thereby releasing heat and triggering spontaneous combustion26.

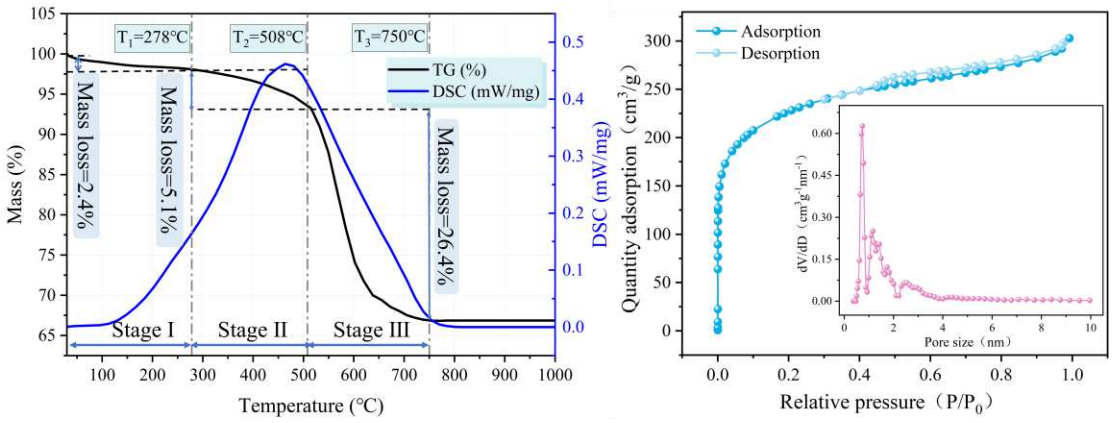


Fig. 6. TG-DSC curves and nitrogen adsorption-desorption isotherms for coal-based activated carbon.

3.2.1 The inhibitory effects of different $Na_2S_2O_8$ concentrations on the various stages of combustion characteristics of coal-based activated carbon

Coal-based activated carbon was subjected to inhibition treatment using $Na_2S_2O_8$ at different concentrations. The TG-DSC curves of the activated carbon were measured using a simultaneous thermal analyzer as the temperature was increased from room temperature to 1000℃, and the inhibitory effect of $Na_2S_2O_8$ on the characteristic stages of the activated carbon's oxidative self-ignition was investigated. Analysis of coal-based activated carbon using thermogravimetric-differential scanning calorimetry revealed that the overall thermal characteristic parameters vary with the concentration of $Na_2S_2O_8$, as shown in Fig. 7(a). As the concentration of the $Na_2S_2O_8$ solution increases, the pyrolysis temperature of the coal-based activated carbon increases continuously. $Na_2S_2O_8$ effectively increases the energy required to decompose the active groups in activated carbon molecules, thereby delaying the pyrolysis process. At the same time, the ignition point temperature showed a trend of first increasing and then decreasing, peaking at a concentration of 5% $Na_2S_2O_8$ solution (541.4℃)—a 33.4℃ increase compared to the ignition point temperature of uninhibited activated carbon. At this concentration, the inhibition treatment was most effective in delaying the onset of violent combustion reactions. At this concentration, the inhibition treatment was most effective in delaying the onset of violent combustion reactions. Under $Na_2S_2O_8$ inhibition treatment, the total heat release decreased. At a 5% $Na_2S_2O_8$ concentration, the total heat release was 1490.6 J/g, a decrease of 67.68 J/g, thereby suppressing the heat generation associated with the spontaneous combustion of activated carbon.

However, when the concentration of the $Na_2S_2O_8$ solution is too high, the pyrolysis temperature continues to rise, but the ignition point temperature drops significantly. Excessively high concentrations of $Na_2S_2O_8$ cause excessive erosion or damage to the pore structure of the activated carbon, allowing oxygen to penetrate more easily into its interior and exposing more active sites, thereby lowering the energy barrier required for ignition.

Fig. 7(b) shows the variation in characteristic parameters for the oxidative heat accumulation and heat storage phases as a function of $Na_2S_2O_8$ concentration. As the concentration of the $Na_2S_2O_8$ solution increases, both weight loss and heat release first decrease and then increase. The weight loss was lowest at a 5% $Na_2S_2O_8$ concentration, at 2.8%, while the heat release decreased from 46.2 J/g to 41.9 J/g. During $Na_2S_2O_8$ inhibition, sulfate radicals preferentially attack and deplete highly active sites while simultaneously removing some surface groups with poor thermal stability. This reduces the number of active sites available for oxidation, thereby lowering the reaction rate and the extent of oxidation, resulting in decreased weight loss and heat release27. Before inhibition, the sustained temperature during the oxidative heat accumulation phase was 248℃; after 5% $Na_2S_2O_8$ inhibition, it decreased to 195.49℃. Since $Na_2S_2O_8$ first consumed the highly active sites on the activated carbon surface and some easily oxidizable functional groups, it reduced the reactivity of the low-temperature oxidation reaction, causing the oxidative heat accumulation phase to end earlier and thereby significantly shortening the sustained temperature range of that phase.

Fig. 7(c) shows the variation of characteristic parameters during the oxidative

pyrolysis phase as a function of $Na_2S_2O_8$ concentration. Under inhibition treatment with $Na_2S_2O_8$ solutions of different concentrations, the weight loss of coal-based activated carbon generally followed a trend of first decreasing and then increasing as the solution concentration rose, while the sustained temperature range and heat release generally followed a trend of first increasing and then decreasing with increasing concentration. After inhibition with a 5% $Na_2S_2O_8$ solution, the weight loss rate reached its minimum, while the heat release and the sustained temperature range over which it occurred reached their maximum. The $Na_2S_2O_8$ inhibition treatment deactivated many active sites on the activated carbon surface and improved the thermal stability of the carbon framework, causing the violent oxidation reaction to occur at higher temperatures and, correspondingly, raising the ignition point temperature. The oxidation rate slowed, heat release became more dispersed, the oxidative pyrolysis phase slowed, and the sustained temperature range widened. When the $Na_2S_2O_8$ concentration was increased to 10% and 15%, excessive oxidation led to the formation of new oxygen-containing functional groups or caused some damage to the pore structure, resulting in a weaker inhibition effect at these concentrations compared to that observed with 5% $Na_2S_2O_8$.

Fig. 7(d) shows how the characteristic parameters of the combustion phase vary with changes in the concentration of $Na_2S_2O_8$. As the concentration of the $Na_2S_2O_8$ solution increases, the heat release of coal-based activated carbon during the combustion phase first decreases and then increases. The coal-based activated carbon treated with a 5% $Na_2S_2O_8$ solution exhibited the lowest heat release, at 1349.7 J/g, representing a decrease of nearly 17% compared to untreated coal-based activated

carbon. Activated carbon subjected to inhibition with 1% and 5% $Na_2S_2O_8$ solutions exhibited significantly lower weight loss than uninhibited activated carbon, and the sustained temperature range was also reduced compared to before inhibition, with the minimum sustained temperature range being 173℃. Low-concentration $Na_2S_2O_8$ solutions first oxidize the more combustible, less stable components on the activated carbon surface, thereby reducing the components that could contribute to exothermic oxidation during the combustion phase. This inhibits the reaction rate, leading to decreases in weight loss, heat release, and the sustained temperature range. When the concentration of the $Na_2S_2O_8$ solution is further increased, excessive oxidation increases the number of oxygen-containing functional groups. During high-temperature combustion, these groups undergo decomposition reactions, releasing additional heat and resulting in more complete combustion, which causes the weight loss, heat release, and sustained temperature range to rise again.

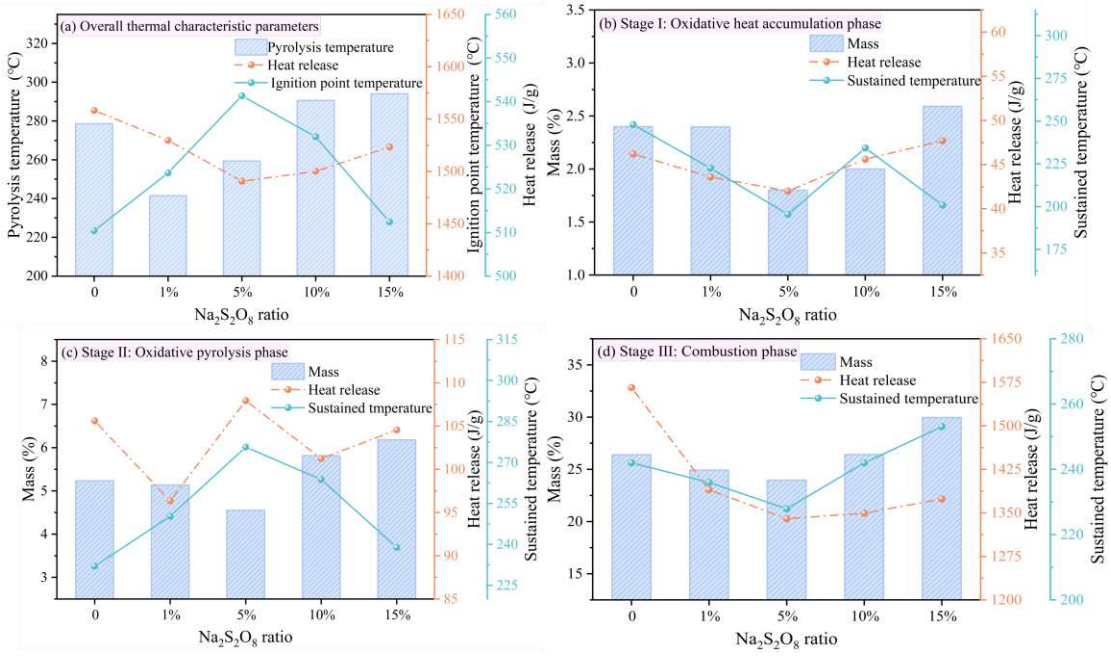


Fig. 7. Characteristic parameters of the various stages of spontaneous

combustion in coal-based activated carbon during the $Na_2S_2O_8$ inhibition process.

3.2.2 Analysis of the effect of different $Na_2S_2O_8$ concentrations on the activation energy of the respective combustion stages of coal-based activated carbon

Activation energy is a measure of the energy required for a chemical reaction to occur; its magnitude directly reflects the reaction's ease or difficulty and the material's thermal stability25. Fig. 8 shows the activation energies for the respective combustion stages of coal-based activated carbon treated with 5% $Na_2S_2O_8$ in the inhibition mode, calculated using the FWO and MKN methods, both of which are based on the constant-conversion-rate approach16, 28. The activation energy increases in stages as the spontaneous reaction proceeds; the later the stage, the higher the energy required, and the more difficult it is for the reaction to proceed. The activation energy for the oxidative heat accumulation phase is shown in Fig. 8(a); as the conversion rate α increases, the apparent activation energy decreases from 74 kJ/mol to 45.2 kJ/mol. During the oxidative heat accumulation phase, the activation energy decreases as adsorbed substances desorb and moisture evaporates; furthermore, because only a small number of active functional groups participate in the reaction, the required activation energy gradually decreases with increasing conversion rate. The activation energy for the oxidative pyrolysis phase is shown in Fig. 8(b). As the reaction progresses, the apparent activation energy decreases as the conversion rate α increases. In the early stages of oxidative pyrolysis, the breaking of strong chemical bonds, such as C–C bonds, requires a higher activation energy. As the reaction proceeds, the reactivity of the generated reaction intermediates increases, and the reaction pathways gradually

simplify, leading to a gradual decrease in activation energy. The activation energy during the combustion phase is shown in Fig. 8(c). During the most vigorous combustion phase, the apparent activation energy decreases from 424.9 kJ/mol to 139.8 kJ/mol. Although the energy barrier is highest during this phase, the combustion reaction becomes more vigorous as the conversion rate α increases, and the activation energy decreases with increasing α.

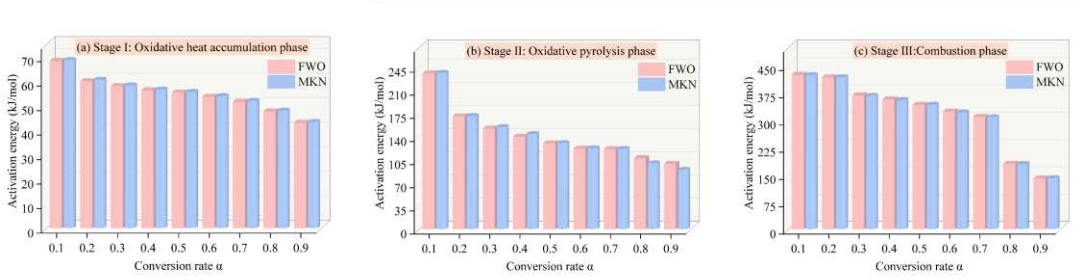


Fig. 8. Comparison of activation energies at various stages for coal-based activated Carbon.

Using the FWO and MKN methods, the experimentally obtained TG-DSC curves were linearly fitted, yielding activation energies for the various characteristic stages of coal-based activated carbon under different $Na_2S_2O_8$ concentrations, as shown in Fig. 9. The activation energy results calculated using the FWO and MKN methods showed little difference; the activation energy of coal-based activated carbon increased as the spontaneous combustion process progressed. The activation energy during the oxidative heat accumulation phase is shown in Fig. 9(a). For coal-based activated carbon treated with an inhibitor, the activation energy ranges from 40 to 60 kJ/mol and first increases, then decreases as $Na_2S_2O_8$ concentration increases, reaching a maximum at 5% $Na_2S_2O_8$ inhibition. The activation energy for the oxidative pyrolysis phase, as

shown in Fig. 9(b), exhibits a trend of first increasing and then decreasing as the concentration of $Na_2S_2O_8$ increases; At lower concentrations of $Na_2S_2O_8$, the compound preferentially acts on unstable oxygen-containing functional groups (such as hydroxyl and aldehyde groups), oxidizing and removing them or converting them into relatively stable functional groups with higher bond energies. This results in the oxidation-pyrolysis reaction having to overcome a higher energy barrier, causing the activation energy to gradually increase29-31. As the concentration of $Na_2S_2O_8$ is further increased, over-oxidation disrupts the structure of the surface-stabilizing functional groups, generating a large number of new oxygen-containing functional groups and unsaturated bonds with low bond energies. This creates reaction pathways that are more prone to low-temperature oxidation, thereby reducing the activation energy required for the reaction—causing the activation energy to first increase and then decrease—and ultimately exhibiting a pattern of first increasing and then decreasing32. As shown in Fig. 9(c), the activation energy during the combustion phase first increases and then decreases with increasing $Na_2S_2O_8$ concentration, reaching a maximum at 5%. Higher concentrations of $Na_2S_2O_8$ alter the pore structure: the decrease in specific surface area and pore volume reduces oxygen adsorption capacity and slows molecular diffusion rates, thereby lowering the activation energy. During the combustion phase, the activation energy of coal-based activated carbon treated with a 5% $Na_2S_2O_8$ solution to inhibit chemical reactions increased significantly, effectively suppressing its tendency toward spontaneous oxidative combustion.

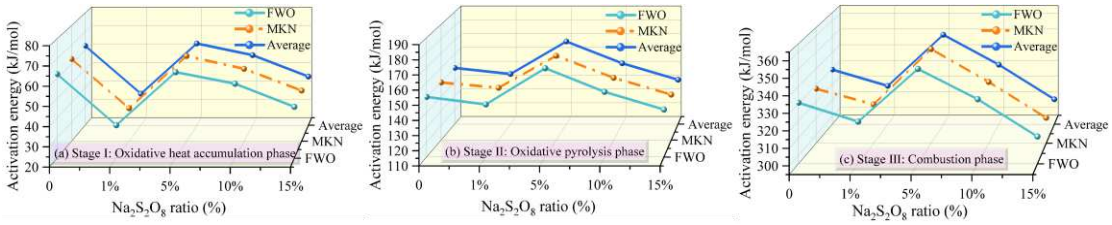


Fig. 9. Comparison of activation energies for different stages of coal-based activated carbon inhibition with $Na_2S_2O_8$ at various concentrations.

3.3 Verification of pore structure changes during the inhibition process of spontaneous combustion in coal-based activated carbon

At different concentrations of $Na_2S_2O_8$ solution, the adsorption-desorption isotherms of the inhibited activated carbon are shown in Fig. 10(a). At all concentrations, the isotherms exhibit characteristics of both Type I and Type IV, indicating adsorption behavior resulting from the synergistic effect of micropores and mesopores. When the concentration of $Na_2S_2O_8$ was low, the adsorption capacity decreased slightly; specifically, at a concentration of 5% $Na_2S_2O_8$, the adsorption capacity was 307.97 cm^3/g, representing a decrease of only 2.44%. The 5% $Na_2S_2O_8$ (low concentration) chemically passivates the highly active sites on the surface of coal-based activated carbon through its oxidizing properties, without damaging the physical framework or pore structure of the activated carbon. When the $Na_2S_2O_8$ concentration was high (10% and 15%), the adsorption capacity of coal-based activated carbon decreased significantly; specifically, the adsorption capacity of activated carbon treated with a 15% $Na_2S_2O_8$ solution was reduced sharply to 193.76 cm^3/g, a 39.88% decrease relative to untreated activated carbon. This indicates that high-concentration $Na_2S_2O_8$ solutions can damage the pore structure of activated carbon, thereby reducing its adsorption

capacity.

The particle sizes of the raw sample and coal-based activated carbon treated at low concentrations (1% and 5%) exhibit a steep and sharp main micropore peak in the <1 nm range, as well as three micropore peaks in the 1-2 nm range. For coal-based activated carbon treated with higher-concentration $Na_2S_2O_8$ solutions (10% and 15%), the peak intensity in the <1 nm region of the particle size distribution decreased significantly; a broad microporous peak was observed in the 1-2 nm region; and the curve flattened out in the 2-10 nm range. For coal-based activated carbon treated with low concentrations (1% and 5%) of $Na_2S_2O_8$, the main micropore peak at 0.7 nm shifted toward larger particle sizes, while the peak intensity remained at a relatively high level. At low concentrations of $Na_2S_2O_8$, the relatively fragile microporous walls on the activated carbon surface were first eroded, resulting in localized oxidative ablation. Under treatment with higher concentrations of $Na_2S_2O_8$, the microporous walls of the coal-based activated carbon underwent severe oxidative ablation, causing adjacent micropores to collapse and resulting in a significant decrease in pore volume.

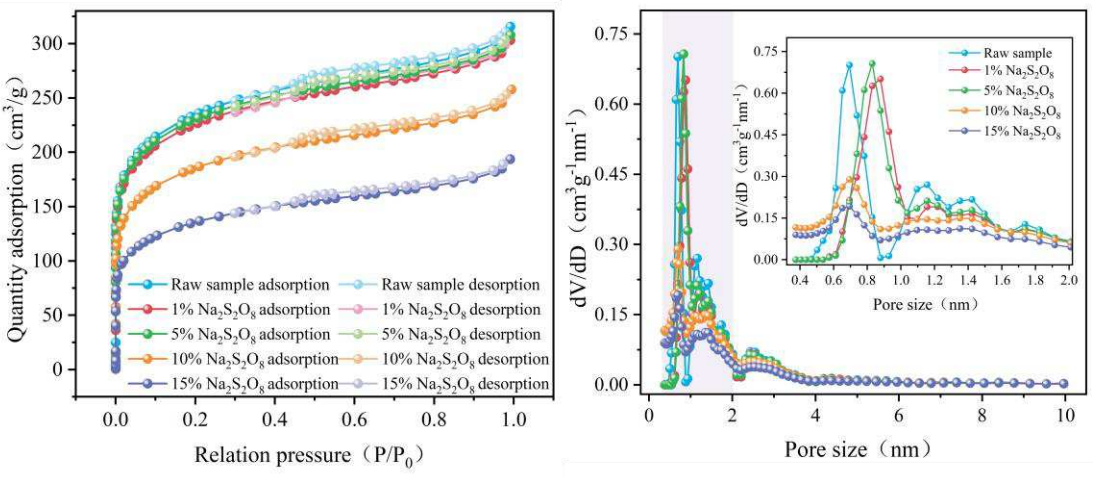


Fig. 10. Nitrogen adsorption-desorption isotherms and particle size distribution

514 curves of coal-based activated carbon treated with an inhibition agent.

515 Fig. 11 shows the pore volume and specific surface area of coal-based activated
516 carbon subjected to inhibition with $Na_2S_2O_8$ at different concentrations. At lower
517 concentrations of $Na_2S_2O_8$ solution (1% and 5%), the pore volume and specific surface
518 area of the activated carbon increase, reaching their maximum values at 5%. When
519 subjected to inhibition with a 5% $Na_2S_2O_8$ solution, the specific surface area of coal-
520 based activated carbon decreased by only 1.87% compared to that before inhibition,
521 and the pore volume decreased by only 2.59%. This indicates that inhibition with a 5%
522 $Na_2S_2O_8$ solution does not damage the pore structure of the activated carbon. However,
523 when the concentration of the $Na_2S_2O_8$ solution was too high (10% and 15%), both the
524 pore volume and specific surface area decreased. Specifically, the pore volume of coal-
525 based activated carbon subjected to inhibition with a 15% $Na_2S_2O_8$ solution decreased
526 by 35.74% compared to that of the untreated sample, and the specific surface area
527 decreased by 39.15%. Under the inhibition of high-concentration $Na_2S_2O_8$, the pore
528 channels of adjacent micropores and mesopores fuse under strong oxidation, forming
529 larger pores with greater particle sizes. Furthermore, high-concentration oxidation tends
530 to form a dense oxide layer at the entrances of micropores, which directly blocks or
531 narrows the pore openings, reducing the number of effective pores and significantly
532 decreasing pore volume and specific surface area.

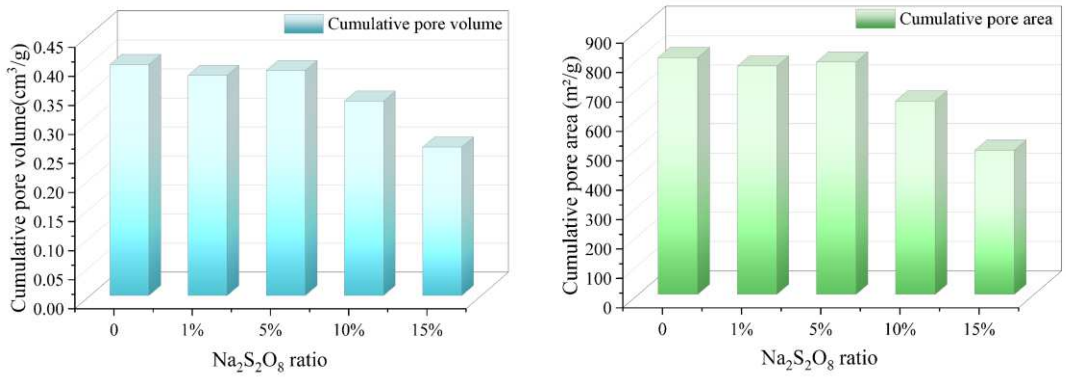


Fig. 11. Pore volume and specific surface area of coal-based activated carbon with different $Na_2S_2O_8$ concentrations.

Fig. 12 shows the distributions of micropore, mesopore, and macropore volumes and specific surface areas of coal-based activated carbon treated with different concentrations of $Na_2S_2O_8$ in the presence of an inhibitor. At low concentrations of $Na_2S_2O_8$, the inhibition effect is primarily concentrated on the active sites on the surface of the activated carbon and within the macropores, while the micropore structure remains relatively intact, and the contribution of the specific surface area remains at a high level (all >80%). At a 5% $Na_2S_2O_8$ concentration, the micropore volume decreased by only 1.71% compared to the state before inhibition, and the specific surface area of the micropores decreased by only 1.6%. Low concentrations of $Na_2S_2O_8$ did not damage the pore structure of the activated carbon. As the concentration of $Na_2S_2O_8$ increased, the microporous and mesoporous structures were disrupted. Specifically, after treatment with a 15% $Na_2S_2O_8$ solution, the microporous pore volume decreased by 40.11% compared to the state before inhibition, and the microporous specific surface area decreased by 40.57%; the mesoporous pore volume decreased by 29.53%, and the mesoporous specific surface area decreased by 32.67%. Under strong oxidative

conditions, adjacent micropores and mesopores fuse to form larger pores; the originally abundant micropore and mesopore structure is destroyed, resulting in a significant decrease in the particle size of the micropores and mesopores, as well as their specific surface area.

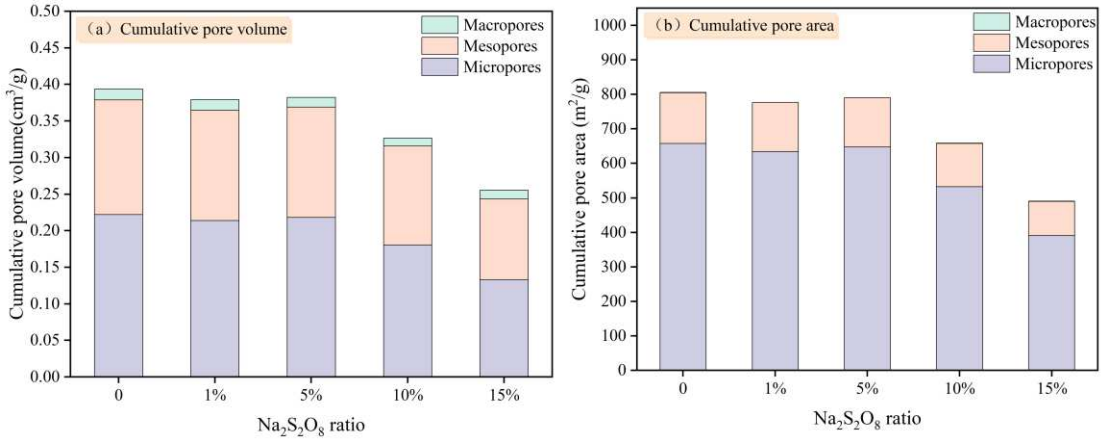


Fig. 12. Distribution of micropore, mesopore, and macropore pore volumes and specific surface areas of coal-based activated carbon at different $Na_2S_2O_8$ concentrations.

4. Conclusions

In this study, bituminous coal from Weining County, Guizhou Province, China, was used as raw material to prepare coal-based activated carbon through carbonization and H_3PO_4/CH_3COOK composite activation pretreatment. Using a fully automated instrument for specific surface area and pore analysis, the study systematically investigated the effects of particle size and activator ratio on the development of the pore structure in coal-based activated carbon. Coal-based activated carbon with the most highly developed pore structure was selected and subjected to inhibition treatment using $Na_2S_2O_8$ solutions of varying concentrations. A comprehensive thermal analyzer

568 was used to analyze the effect of $Na_2S_2O_8$ inhibition on the suppression of the
569 characteristic stages of spontaneous combustion in the deactivated coal-based activated
570 carbon. Combining kinetic methods such as FWO and MKN, the influence of $Na_2S_2O_8$
571 concentration on the activation energy of the characteristic stages of oxidative
572 spontaneous combustion in coal-based activated carbon was investigated. A fully
573 automated specific surface area and pore structure analyzer was used to study the pore
574 structure of coal-based activated carbon with good flame-retardant properties, to verify
575 changes in pore structure during the inhibition of its spontaneous combustion using
576 $Na_2S_2O_8$. The main conclusions are as follows:

577 1） The adsorption capacity of activated carbon increases significantly as particle
578 size decreases and follows a trend of initially increasing and then decreasing
579 with an increase in the H_3PO_4/CH_3COOK mass ratio. Specifically, within the
580 particle size range of 0.074–0 mm, the pore structure is most well-developed,
581 the adsorption capacity is highest, and the pore volume and specific surface
582 area are largest when the H_3PO_4/CH_3COOK mass ratio is 1:3. The increase in
583 pore volume and specific surface area stems from the growth of micropores and
584 mesopores. When the H_3PO_4/CH_3COOK ratio is too high, some micropores
585 and mesopores merge or undergo localized pore degradation, thereby reducing
586 the pore volume and specific surface area of the micropores and mesopores.

587 2） $Na_2S_2O_8$ effectively suppresses the spontaneous combustion tendency of coal-
588 based activated carbon; a 5% $Na_2S_2O_8$ concentration provides the best
589 inhibition, raising the ignition point temperature by 33.4℃ and reducing the

total heat release by 67.68 J/g. During the oxidative heat accumulation phase, as the $Na_2S_2O_8$ concentration increased, both weight loss and heat release first decreased and then increased, while the activation energy first decreased; with 5% $Na_2S_2O_8$, heat release and weight loss reached their minimum values, while activation energy reached its maximum value. During the oxidative pyrolysis phase, inhibition treatment significantly deactivates active sites on the surface of activated carbon and improves the thermal stability of the carbon framework. As a result, violent oxidative reactions occur at higher temperatures, and the ignition point temperature rises accordingly; the activation energy reaches its maximum value after inhibition treatment with 5% $Na_2S_2O_8$. A low-concentration $Na_2S_2O_8$ solution first oxidizes the flammable, unstable components on the surface of the activated carbon, thereby reducing the number of components that can contribute to exothermic oxidation during combustion. This leads to a decrease in weight loss, heat release, and the sustained temperature range, and the activation energy during the combustion phase also reaches its maximum value after inhibition with a 5% $Na_2S_2O_8$ retardant.

3） 5% $Na_2S_2O_8$ can maintain a high adsorption capacity while passivating active sites; however, excessively high concentrations can cause adjacent micropores and mesopores to coalesce under strong oxidative conditions, destroying the pore structure of the activated carbon and significantly decreasing adsorption capacity. During the inhibition treatment, 5% $Na_2S_2O_8$ did not damage the

original pore structure of the coal-based activated carbon, and the activated carbon retained its high adsorption performance.

Funding This work was financially supported by National Natural Science Foundation of China (grant numbers 52370142, 52070127 and 52270129), Oriental Talent Youth Program, Shanghai Shuguang Program (23SG52), Guizhou Provincial Key Technology R&D Program (QKHZC(2024)153). The authors are thankful for all of the support for this research.

Author contributions Qin Xu: Writing - review & editing, Writing - original draft, Methodology, Investigation. Yiping Tan: Writing - review & editing, Data curation. Jie Guan: Resources, Methodology. Hao Yuan: Resources, Data curation, Conceptualization. Shengqiang Yang: Resources, Conceptualization. Yaoguang Guo: Resources, Data curation, Conceptualization.

Data availability The data that support the findings of this study are available from the corresponding author, upon reasonable request.

Declarations

Ethical approval The authors declare that there are no human cells and tissues are used in this manuscript.

Competing interests The authors declare no competing interests.

References

1 Y. Zhu, H. Liu, T. Wang, Y. Wang, H. Liu, Evolution of pore structures and fractal characteristics of coal-based activated carbon in steam activation based on nitrogen adsorption method, Powder Technology, 424 (2023).http://dx.doi.org/10.1016/j.powtec.2023.118522

2 C. Li, Y. Wang, C. Zhang, Y. Zhou, J. Jing, J. Shen, J. Li, J. Yang, Enhancing CH4/N2 adsorption and separation performance of low-rank coal-based porous carbon by pyrolytic pretreatment, Fuel, 428 (2027).http://dx.doi.org/10.1016/j.fuel.2026.140293

3 L. Li, S. Luo, C. Deng, X. Tian, S. Yan, Y. Zhang, Optimization of K2CO3 green activation of lignite for high-performance porous carbon and its application in supercapacitors, Journal of Energy Storage, 164 (2026).http://dx.doi.org/10.1016/j.est.2026.122202

4 L. Dong, Q. Xu, Y. Yao, Y. Han, G. Zhang, Utilization of Coal-Based Activated Carbon (JA) for the Adsorption of Methyl Orange Azo Dye in Wastewater, Water, 18 (2026).http://dx.doi.org/10.3390/w18020289

5 D.-G. Kim, T.-H. Kim, S.-O. Ko, Enhanced Catalytic Activity of a Coal-Based Powdered Activated Carbon by Thermal Treatment, Water, 14 (2022).http://dx.doi.org/10.3390/w14203308

6 W. Spencer, G. Senanayake, M. Altarawneh, D. Ibana, A.N. Nikoloski, Review of the effects of coal properties and activation parameters on activated carbon production and quality, Minerals Engineering, 212 (2024).http://dx.doi.org/10.1016/j.mineng.2024.108712

7 C. Zhao, L. Ge, L. Mai, X. Li, S. Chen, Q. Li, S. Li, L. Yao, Y. Wang, C. Xu, Review on Coal-Based Activated Carbon: Preparation, Modification, Application, Regeneration, and Perspectives, Energy & Fuels, 37 (2023) 11622-11642.http://dx.doi.org/10.1021/acs.energyfuels.3c01866

8 Y. Li, Z. Yu, J. Guo, X. Li, F. Yang, B. Zhang, Ultrasonic-assisted water washing dechlorination modified coal-based activated carbon and its adsorption performance for dyes, Journal of Cleaner Production, 546 (2026).http://dx.doi.org/10.1016/j.jclepro.2026.147735

9 Y. Yang, M. Li, X. Zhang, D. Liu, J. Jeong, L. Peng, J. Zuo, Coal-based activated carbon for low-carbon cement mortars: Multiscale mechanisms governing mechanical behavior, Construction and Building Materials, 509 (2026).http://dx.doi.org/10.1016/j.conbuildmat.2026.145101

10 X. Gao, Y. Ju, G. Hou, C. Liu, Efficient treatment of coking wastewater by coal-based activated carbon prepared through coal blending method, Colloids and Surfaces a-Physicochemical and Engineering Aspects, 705 (2025).http://dx.doi.org/10.1016/j.colsurfa.2024.135675

11 Y. Xiao, H.-M. Zhang, L. Yin, C.-M. Shu, Q.-W. Li, Spontaneous Combustion Risk of Coal-based Activated Carbon, Combustion Science and Technology, Vol.195 (2023) 47-63.http://dx.doi.org/10.1080/00102202.2021.1933961

12 L. Wang, Q. Fan, Y. Wang, Y. Xu, Y. Li, Y. Zheng, X. Feng, K. Zhang, Study on Thermal Risk of Coal-Based Activated Carbon after Adsorbing Acetone, Cyclohexane, and Butyl Acetate, Acs Omega, 8 (2023) 33883-33890.http://dx.doi.org/10.1021/acsomega.3c04577

13 J. Li, W. Zhou, J. Li, N. Xue, X. Meng, L. Xie, Y. Yu, Z. Liu, Z. Qu, J. Gao, F. Sun, G. Zhao, Efficient production of activated carbon with well-developed pore structure based on fast pyrolysis-physical activation, Journal of the Energy Institute, 115 (2024).http://dx.doi.org/10.1016/j.joei.2024.101685

14 Z. Qie, X. Zhang, Z. Wang, Z. Liu, H. Alhassawi, H. Li, G. Chen, G. Zhao, Effect of pretreatment and activation conditions on pore development of coal-based activated carbon, Journal of Industrial and Engineering Chemistry, 139 (2024) 611-619.http://dx.doi.org/10.1016/j.jiec.2024.05.037

15 W. Spencer, D. Ibana, P. Singh, A.N. Nikoloski, Effect of Surface Area, Particle Size and Acid Washing on the Quality of Activated Carbon Derived from Lower Rank Coal by KOH Activation, Sustainability, 16 (2024).http://dx.doi.org/10.3390/su16145876

16 Y. Xiao, K.-H. Liu, P. Pang, C.-M. Shu, Thermokinetics behaviour and parameters for spontaneous combustion of carbonised powders and oxidised powders from preparation of coal-based activated carbon, Journal of Thermal Analysis and Calorimetry, 144 (2021) 415-424.http://dx.doi.org/10.1007/s10973-020-10441-3

17 H.-F. Lyu, F.-X. Shen, Y. Li, C.-P. Wang, J. Deng, W.-F. Wang, Research on spontaneous combustion thermal generation and transfer effects of coal-based activated carbon and its precursors, Process Safety and Environmental Protection, 209 (2026).http://dx.doi.org/10.1016/j.psep.2026.108578

18 S. Shimizu, N. Matubayasi, Sorption: A Statistical Thermodynamic Fluctuation Theory, Langmuir, 37 (2021) 7380-7391.http://dx.doi.org/10.1021/acs.langmuir.1c00742

19 T. Chi, W. Zeng, D. Xie, C. Wang, S. Li, Z. Tang, Z. Yuan, High-purity porous carbon via synergistic PTFE etching/KOH activation for efficient iodine capture, Chemical Engineering Journal, 529 (2026).http://dx.doi.org/10.1016/j.cej.2026.172789

20 K. Rahbar-Shamskar, P.A. Azar, A. Rashidi, S. Baniyaghoob, M. Yousefi, Synthesis of micro/mesoporous carbon adsorbents by in-situ fast pyrolysis of reed for recovering gasoline vapor, Journal of Cleaner Production, 259 (2020).http://dx.doi.org/10.1016/j.jclepro.2020.120832

21 Y. Zhai, Y. Li, D. Song, J. Pan, Gas Diffusion Characteristics and Size Effect in Coal Particles with Different Degrees of Metamorphism, Energy & Fuels, 37 (2023) 2030-2039.http://dx.doi.org/10.1021/acs.energyfuels.2c03865

693 22 A. Korus, J. Jagiello, H. Jaroszek, P. Copik, A. Szlek, Variation of pore development scenarios by
694 changing gasification atmosphere and temperature, Energy, 289
695 (2024).http://dx.doi.org/10.1016/j.energy.2023.129897
696 23 C. Wedler, R. Span, A pore-structure dependent kinetic adsorption model for consideration in char
697 conversion - Adsorption kinetics of CO2 on biomass chars, Chemical Engineering Science, 231
698 (2021).http://dx.doi.org/10.1016/j.ces.2020.116281
699 24 R. Xu, X. Xian, Z. Song, M. Gu, The impact of effective pore percentage on CH4/N2 separation in
700 coal-based activated carbon, Journal of Materials Science, 58 (2023) 13635-
701 13648.http://dx.doi.org/10.1007/s10853-023-08869-7
702 25 L. Ge, C. Zhao, S. Chen, Q. Li, T. Zhou, H. Jiang, X. Li, Y. Wang, C. Xu, An analysis of the
703 carbonization process and volatile-release characteristics of coal-based activated carbon, Energy,
704 257 (2022).http://dx.doi.org/10.1016/j.energy.2022.124779
705 26 Q. Xu, L. Huang, J. Guan, S. Yang, W. Dong, Y. Guo, Y. Wu, Z. Chen, X. Zhang, S. Chen, Kinetic
706 and thermal effect of various stages in the process of coal-based activated carbon spontaneous
707 combustion after activation pretreatment, Fuel, 413
708 (2026).http://dx.doi.org/10.1016/j.fuel.2025.138197
709 27 Z. Xia, T. Deng, C. Song, J. Li, Decarboxylative sulfation by persulfates, Chemical Science, 16
710 (2025) 11568-11573.http://dx.doi.org/10.1039/d5sc03129j
711 28 T. Zhao, S. Yang, X. Hu, W. Song, J. Cai, Q. Xu, Restraining effect of nitrogen on coal oxidation in
712 different stages: Non-isothermal TG-DSC and EPR research, International Journal of Mining
713 Science and Technology, 30 (2020) 387-395.http://dx.doi.org/10.1016/j.ijmst.2020.04.008

29 X. Huang, Y. Xu, Y. Wang, Y. Li, L. Wang, Z. Wu, Are Ionic Liquids Suitable for Suppressing Coal Spontaneous Combustion?, Acs Omega, 6 (2021) 6681-6690.http://dx.doi.org/10.1021/acsomega.0c05504

30 C. Wang, Y. Xiao, Q. Li, J. Deng, K. Wang, Free radicals, apparent activation energy, and functional groups during low-temperature oxidation of Jurassic coal in Northern Shaanxi, International Journal of Mining Science and Technology, 28 (2018) 469-475.http://dx.doi.org/10.1016/j.ijmst.2018.04.007

31 G. Bai, H. Xin, P. Zhang, C. Luo, J. Li, Q. Zeng, B. Genc, M. Onifade, D. Wang, Study on functional group evolution mechanisms and chemical kinetics during gas coal oxygen-free pyrolysis: Insights from high-temperature in-situ FTIR, Journal of Cleaner Production, 529 (2025).http://dx.doi.org/10.1016/j.jclepro.2025.146801

32 S. Lu, J. Zhao, J. Song, J. Chang, C.-M. Shu, Apparent activation energy of mineral in open pit mine based upon the evolution of active functional groups, International Journal of Coal Science & Technology, 10 (2023).http://dx.doi.org/10.1007/s40789-023-00650-0